Phase diagrams of vortex matter with multi-scale inter-vortex interactions in layered superconductors

2017 J. Phys.: Condens. Matter 29 035602

(http://iopscience.iop.org/0953-8984/29/3/035602)

IOP Publishing Journal of Physics: Condensed Matter

J. Phys.: Condens. Matter **29** (2017) 035602 (16pp) doi:10.1088/1361-648X/29/3/035602

Phase diagrams of vortex matter with multi-scale inter-vortex interactions in layered superconductors

Qingyou Meng[1], Christopher N Varney[2], Hans Fangohr[3] and Egor Babaev[4]

[1] Department of Physics, University of Massachusetts, Amherst, MA 01003, USA
[2] Department of Physics, The University of West Florida, Pensacola, FL 32514, USA
[3] Engineering and the Environment, University of Southampton, SO17 1BJ, UK
[4] Department of Theoretical Physics, The Royal Institute of Technology, SE-10691 Stockholm, Sweden

E-mail: babaev@kth.se

Received 1 August 2016, revised 24 October 2016
Accepted for publication 25 October 2016
Published 16 November 2016

Abstract

It was recently proposed to use the stray magnetic fields of superconducting vortex lattices to trap ultracold atoms for building quantum emulators. This calls for new methods for engineering and manipulating of the vortex states. One of the possible routes utilizes type-1.5 superconducting layered systems with multi-scale inter-vortex interactions. In order to explore the possible vortex states that can be engineered, we present two phase diagrams of phenomenological vortex matter models with multi-scale inter-vortex interactions featuring several attractive and repulsive length scales. The phase diagrams exhibit a plethora of phases, including conventional 2D lattice phases, five stripe phases, dimer, trimer, and tetramer phases, void phases, and stable low-temperature disordered phases. The transitions between these states can be controlled by the value of an applied external field.

Keywords: multi-scale interaction, vortex matter, type 1.5 superconductor, layered superconductor, vortex phases, phase diagram

(Some figures may appear in colour only in the online journal)

1. Introduction

Recently much interest was generated by the proposal of quantum systems built by placing ultracold atoms in a lattice potential generated via stray magnetic fields of superconducting vortices [1]. This gives rise to a possibility of creating quantum emulators. To this end, better control of vortex lattices in superconductors is required. Predominantly vortex lattices in superconductors have hexagonal symmetry, the square lattices are possible but rare [2–4].

One route for creating more complicated vortex lattices is through pinning the vortices by artificial pinning centers [5–11]. This approach, demonstrated by Romero *et al* in [1], appears technically challenging to achieve the requirements for perfections of the vortex lattice due to possible variations and field inhomogeneities in the anti-dot arrays.

In [12], an alternative approach was proposed that involves multi-component superconducting type-1.5 superconducting systems. In such systems, there are several coherence lengths that can be smaller and/or larger than the penetration length (we absorb a factor of $2^{-1/2}$ in the definition of coherence length): $\xi_1, \xi_2, \ldots < \lambda < \xi_i, \ldots, \xi_N$ [13–19]. The first claim of experimental observation of this behavior was originally reported in works on MgB_2 [20–22]. Recently a similar claim was reported in experimental studies of Sr_2RuO_4 [4, 23] and $LaPt_3Si$ [24, 25]. The non-monotonic inter-vortex interaction is also possible in electromagnetically or proximity-effect-coupled bilayers [13].

In case of two-component superconductors, the long-range inter-vortex interaction energy is given by [13, 14, 26]

$$E_{\rm int} = C_B^2 K_0\left(\frac{r}{\lambda}\right) - C_1^2 K_0\left(\frac{r}{\xi_1}\right) - C_2^2 K_0\left(\frac{r}{\xi_2}\right). \qquad (1)$$

Here, the first term describes inter-vortex repulsion which comes from magnetic and current–current interaction and has the length scale of magnetic field penetration length. The second and third terms describes attractive interactions from cores overlaps with ranges set by coherence lengths. Multiple repulsive length scales can arise in layered systems due to different penetration lengths in different layers or due to splaying of magnetic field in interlayer spacing of superconductor-insulator-superconductor systems. In such systems with multiple repulsive length scales, a variety of cluster phases are possible due to the combination of multi-scale repulsive interactions with attractive ranges [27]. Some of the phases obtained in [27] were also reproduced in simulations of a layered Ginzburg–Landau model [28]. In [12], it was discussed that these models also allow vortex lattices with different symmetries. However a phase diagram of these models has not been investigated previously.

In what follows, we will discuss the phenomenological model used in this study in section 2. In section 3, the details of the simulation method and measurements used to characterize each phase are described. In section 4, we present two phase diagrams featuring 10 and 17 phases, respectively, and characterize each phase. Discussion of the especially interesting phases in both phase diagrams is in section 5. Finally, the impact of the results are discussed in section 6.

2. Model

Motivated by the multi-scale character of intervortex interaction in type-1.5 systems, here we study a phase diagram of a prototypical system with N_v vortices exhibiting multi-scale inter-vortex interactions. The effective model for a vortex under these conditions can be described by using a hard-core radius σ_h, an inner soft-core radius σ_1, and an outer soft-core radius σ_2. In addition, we can account for the effect of stray fields, which give an effective power-law interaction [29]. To generate such potentials, we define the potential energy using a phenomenological model [12, 27]

$$\frac{V(r)}{V_0} = \mathrm{e}^{-r/\lambda} - c_2\mathrm{e}^{-r/\xi} + c_3\frac{\lambda\{\tanh[a(r-b)]+1\}}{r+\delta} \qquad (2)$$

where V_0 defines arbitrary unit of energy and λ and ξ play the role of the penetration and larger coherence lengths. We set $\lambda = 1$ to set the unit of length and refer to all distances in terms of λ. The constants c_2, c_3, a, b, and δ are phenomenological coefficients. In order to get a potential qualitatively similar to equation (1) with the addition of a long-range interaction caused by stray fields, we set $c_2 = 0.2$, $c_3 = 0.1$, and $\delta = 0.1$. In order to control the short-range repulsive length scale of the inter-vortex potential, we tune a, b and the ratio ξ/λ.

The three terms in equation (2) are a short-range repulsive interaction, an intermediate attractive interaction, and a long-range repulsive interaction caused by stray fields [29]. In the denominator of the third term, the parameter δ removes the hard core of the vortex interaction, i.e. $\sigma_h = 0$, and reduces the impact of the short-range repulsive interaction caused by power-law term. For other contexts where multi-scale interparticle interactions arise see [30–37].

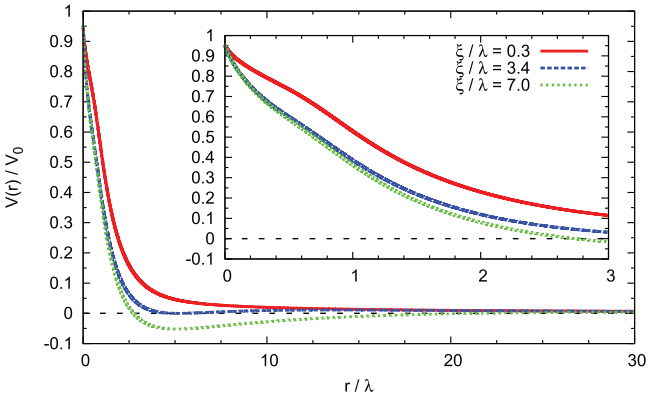

Figure 1. Inter-vortex pair potentials at $a = 2.5$, $b = 0.5$ and $\xi/\lambda = 0.3$, 3.4, and 7.0. When $0.5 \leqslant \xi \leqslant 3.4$, there is only purely repulsive interactions in the potential. When $3.4 < \xi \leqslant 10.0$, the potential has the attractive well around $r/\lambda \approx 5.2$.

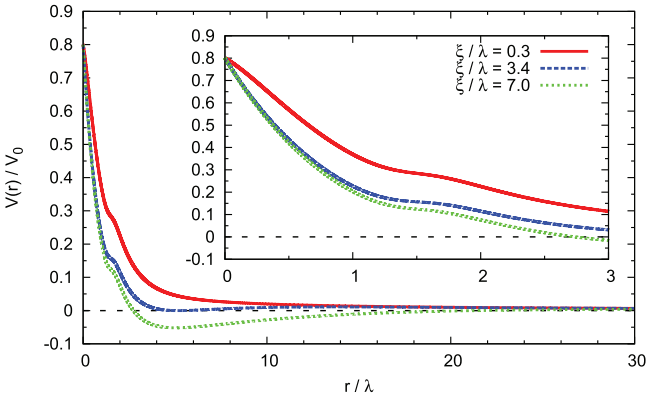

Figure 2. Inter-vortex pair potentials at $a = 3.0$, $b = 1.5$ and $\xi/\lambda = 0.3$, 3.4, and 7.0. Similarly as figure 1, when $\xi > 3.4$, there is one attractive well around $r/\lambda \approx 5.2$ at the potential.

In this work, we consider two series of potentials. In the first, shown in figure 1, $a = 2.5$, $b = 0.5$, and ξ/λ ranges from 0.2 to 10.0. In the second, shown in figure 2, $a = 3.0$, $b = 1.5$, and ξ/λ varies from 0.1 to 10.0. In both figures 1 and 2, we show three typical potentials by changing the ratio of the length scales ξ/λ. Note that as ξ/λ increases, the attractive region of the potentials are enhanced.

The solid red lines in figures 1 and 2 represent a typical potential form at small ξ values($\xi/\lambda = 0.3$), which contains three short-range repulsive length scales and one long-range repulsive length scale. The dashed blue lines in figures 1 and 2 are for a potential at $\xi/\lambda = 3.4$, which has a minimum $V(r)/V_0 = 0$ at $r/\lambda \approx 5.2$. From $\xi/\lambda = 3.4$ to 10.0, there is one attractive well in the potential and the attractive short length increases as the ξ increases. The dotted green line in figures 1 and 2 represent a potential at $\xi/\lambda = 7.0$, which has an attractive well.

3. Simulation method

We utilize Langevin dynamics [38] with simulated annealing to calculate the ground state of this vortex system. The overdamped Langevin equation of motion for a vortex at $\mathbf{r}_i$ is

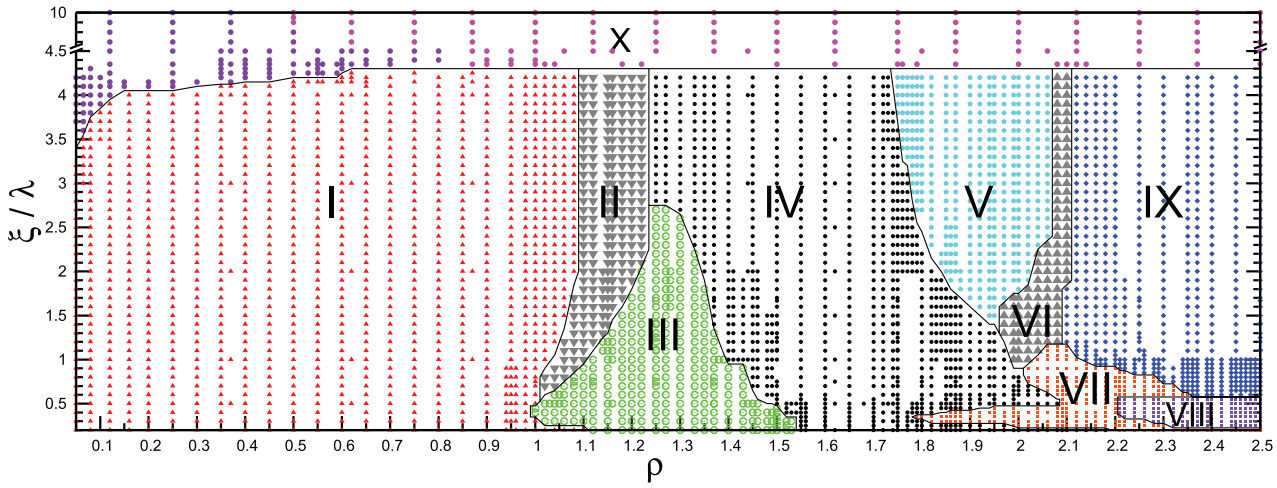

Figure 3. Phase diagram of the final vortex configuration at zero temperature in the ξ/λ-ρ plane for the potential shown in figure 1. For each point, $N_v = 780$ was used in the simulation with the exception of phases I and IV, which used $N_v = 986$ and $N_v = 4012$, respectively. Representative vortex configurations for each phase are shown in figure 4.

$$\mathbf{F}_i = \sum_{j\neq i}^{N_v} \mathbf{F}^{vv}(\mathbf{r}_i - \mathbf{r}_j) + \mathbf{F}_i^T = \eta \frac{\mathrm{d}\mathbf{r}_i}{\mathrm{d}t} \tag{3}$$

where $\mathbf{F}_i$ is the total force on vortex i, $\mathbf{F}^{vv}(\mathbf{r}_i - \mathbf{r}_j) = -\nabla V_{ij}$ is the inter-vortex force between vortices i and j, N_v is the number of vortices, $\mathbf{F}_i^T$ is the stochastic thermal force, η is the friction coefficient.

We do our simulation within a nearly square $L_x \times L_y$ box and employ the periodic boundary conditions. We used random initial configurations for each simulation and compared with a perfect hexagonal lattice. In order to get the perfect initial hexagonal lattice, L_x and L_y are chosen to alleviate the effects of frustration [38] and keep $L_x/L_y \approx 1$. The density is defined as $\rho = \frac{N_v}{L_x L_y}$, where N_v is the number of vortices. In the phase diagrams shown, the number of vortices were $N_v = 780$ and 986 at low and high density, respectively. In addition, the existence of each phase was verified with simulations of at least $N_v = 2958$ vortices.

In order to characterize each phase, we first considered the radial distribution function (RDF)

$$g(r) = \frac{1}{2\pi r \Delta r \rho N_v} \sum_{i=1}^{N_v} n_i(r, \Delta r), \tag{4}$$

where $n_i(r, \Delta r)$ is the number of particles in the shell surrounding the ith vortex with radius r and thickness Δr. The RDF is used to characterize the structure of a configuration. For small separations, $g(r) = 0$ and as $r \to \infty$ $g(r) \to 1$. In the RDF, sharp peaks are a clear signature of ordering into shells of nearest neighbors while peak broadening is an indication of a breakdown in long-range order. An absence of well-defined peaks is a clear signature of local structure only.

Next, we considered the static structure factor [39]

$$S(\mathbf{k}) = \frac{1}{N}\left\langle \left(\sum_i^N \cos(\mathbf{k}\cdot\mathbf{r}_i)\right)^2 + \left(\sum_i^N \sin(\mathbf{k}\cdot\mathbf{r}_i)\right)^2 \right\rangle \tag{5}$$

to characterize the intermediate and large scale structure of the vortex configurations. Here $\mathbf{k} \equiv (k_x, k_y)$, $k_{x(y)} = n_{x(y)} k_{0x(0y)}$ and $k_{0x(0y)} = 2\pi/L_{x(y)}$. In our simulations, $L_x \approx L_y$, so $k_{0x} \approx k_{0y}$ and we use k_{0x} as the unit of scale.

The final measures we use to define the structure is the number of nearest neighbors n_1 and the nearest-neighbor distance r_1. The number of nearest neighbors n_1 is determined by counting the average number of vortices within circle of radius $r_{\min}$ where $r_{\min}$ is the distance corresponding to the minimum value between the first and second peak in the RDF. The nearest neighbor distance r_1 is defined by the location of the first maximum in $g(r)$.

While ordered phases will have clear signatures in $g(r)$, $S(\mathbf{k})$, and n_1, disordered phases will not exhibit long-range order and are characterized by a uniform ring structure in $S(\mathbf{k})$ and lack of symmetry breaking. Phases that have these characteristics in the structure factor will be referred to as as disordered or 'glassy' phase (we do not discuss dynamic characterisation of glassiness in this paper).

4. Results

4.1. Phase diagram I

The ground state phase diagram in the density ρ and ξ/λ plane corresponding to figure 1 is shown in figure 3. Here, we set $a = 2.5$, $b = 0.5$. The density is varied from $\rho = 0.05$ to 2.50 and ξ/λ ranges from 0.2 to 10.0. The phase diagram exhibits 10 different phases and representatives of each phase are illustrated in figure 4, where each phase is represented by a different symbol. Phase I is a hexagonal lattice (solid red up-pointing triangle), phase III is a dimer lattice (green circle), and phase IV is a stripe phase (solid black circle). Phase V is a honeycomb lattice (solid cyan pentagon), phase VII is a polarized triangular trimer (solid orange square), phase VIII is a tetramer lattice (solid purple square), and phase IV is a kagomé lattice (solid blue rhombus). Phase X is a cluster phase featuring multiple clusters (solid violet circle) for smaller densities and ξ/λ and single giant clusters (solid

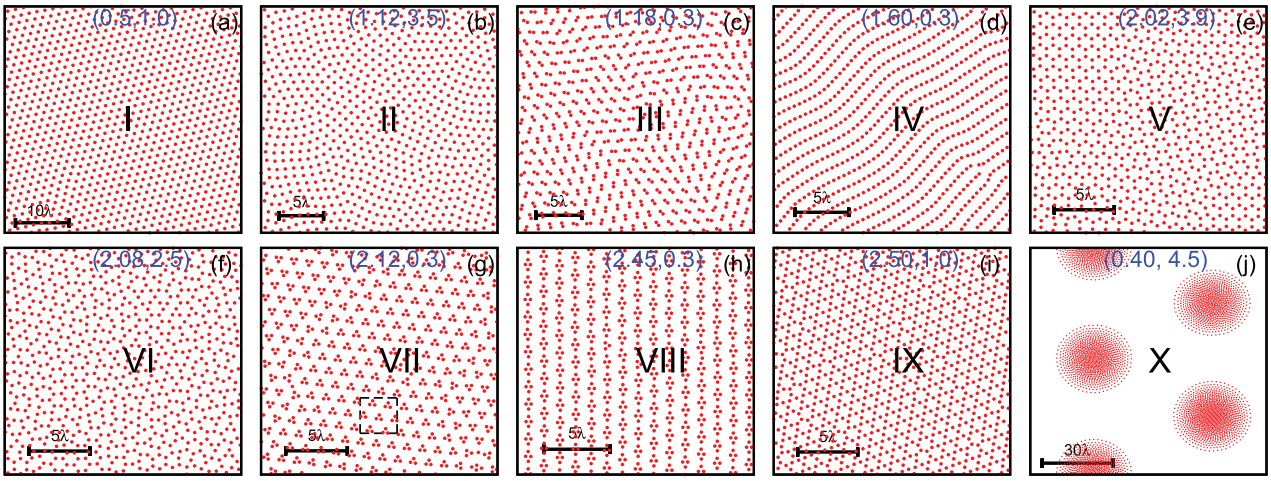

Figure 4. Snapshot of a representative vortex configuration for each phase (indicated by Roman numerals) in figure 3. The coordinate of the phase diagram $(\rho, \xi/\lambda)$ is indicated on each panel.

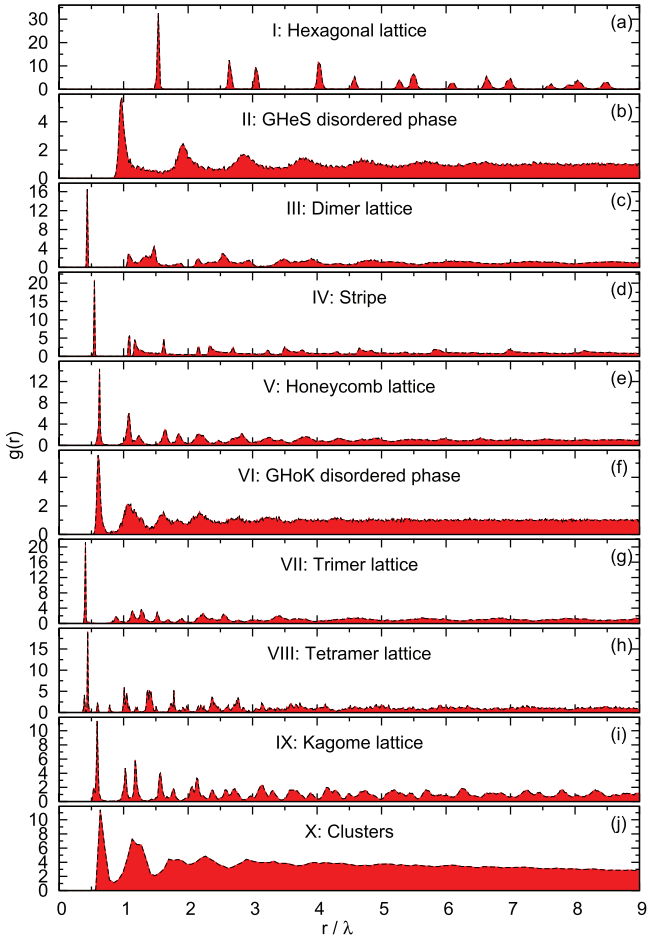

Figure 5. Radial distribution functions $g(r)$ corresponding to the phases illustrated in figure 4.

pink circle) for larger densities and ξ/λ. Phases II and VI are disordered states (solid dark gray down-pointing and up-pointing triangles, respectively). Phase II separates the hexagonal lattice and stripe phases while phase VI is bordered by the honeycomb and kagome lattice phases. Consequently, we shall distinguish these two states as GHeS and GHoK, which is an combination of the phases that border the disordered phases.

Figure 4 shows a snapshot of a representative state for every phase in figure 3. The corresponding radial distribution functions $g(r)$ and static structure factors $S(\mathbf{k})$ are shown in figures 5 and 6, respectively. The number of the nearest neighbors n_1 in each phase and the nearest neighbor distance are shown in figures 7 and 8, respectively, for various ξ/λ to show how each quantity changes along all of the phase transitions figure 3. In figures 7 and 8, the background colors correspond to different phases: white (hexagonal lattice), gray (disordered 'glassy' phases), green (dimer lattice), black (stripe), cyan (honeycomb lattice), orange (trimer lattice), purple (tetramer lattice) and blue (kagome lattice). Note that the gray regions corresponding to both disordered phases, with the GHeS phase at $\rho \approx 1.00$ and GHoK at $\rho \approx 2.00$. Here we show the n_1 for $\xi = 0.3$, 0.7, 1.0, 1.3, and 3.0, which is sufficient to show all of the phase transitions in figure 3.

Let us first consider the phases that exhibit long-range order. For $\xi/\lambda < 3.5$ and $\rho = 0.05$ to $\rho \approx 1.00$, the ground state of the system is a hexagonal lattice (phase I in figure 3). A typical ground state configuration is shown in figure 4(a) and corresponds to $\rho = 0.50$ and $\xi/\lambda = 1.0$. This phase is characterized by sharp peaks in $g(r)$ located at distances corresponding to the neighbor distances of a hexagonal lattice and a sharply defined hexagonal structure in $S(\mathbf{k})$, which are shown in figures 5(a) and 6(a), respectively. Another confirmation of the structure can be found in figure 7, where the hexagonal lattice is indicated by a white background and has $n_1 = 6$. The prevalence of this phase at low densities is largely driven by the long-range repulsive interaction caused by stray-fields.

Next, for small ξ/λ and densities ranging from $\rho = 1.0$ to $\rho = 1.5$, vortices continue to form a hexagonal lattice but individual vortices pair to form dimers (phase III). A typical snapshot of a dimer lattice ($\rho = 1.18$ and $\xi/\lambda = 0.3$) is shown in figure 4(c), where there is some alignment of the dimers but domains form for smaller ρ and ξ/λ. This phase is similar to the dimer phase observed in potentials with two repulsive length scales [30–33]. In $g(r)$, see figure 5(c), the location of the first peak is at $r/\lambda = 0.44$ while the first peak of the hexagonal lattice is at $r/\lambda = 0.99$[5]. Moreover,

[5] The hexagonal lattice order a can be calculated given the density ρ. The relation between them is $\rho = (\sqrt{3}a^2/2)^{-1}$. Then we can get $a = \sqrt{2/(\sqrt{3}\rho)}$. If $\rho = 1.12$, then $a = 1.02$; $\rho = 1.18$, then $a = 0.99$.

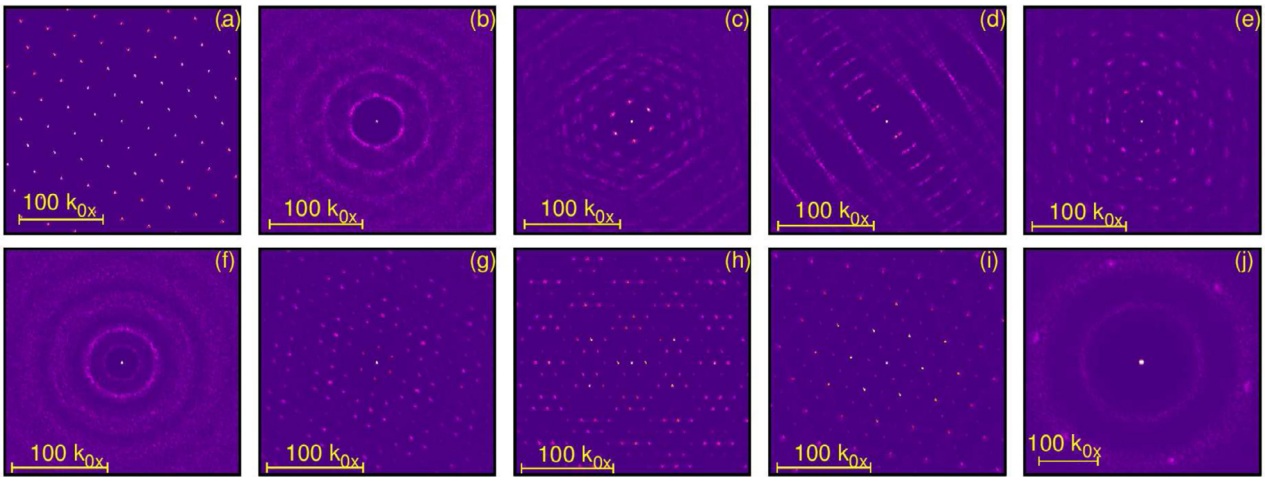

Figure 6. Static structure factor $S(\mathbf{k})$ corresponding to the phases illustrated in figure 4.

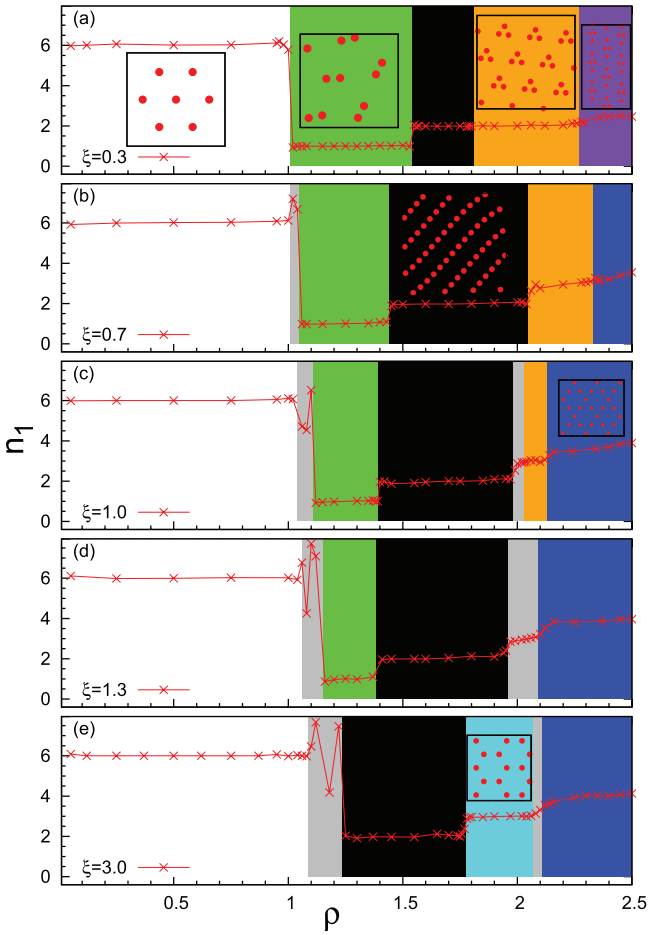

Figure 7. Nearest neighbor number n_1 at: (a). $\xi = 0.3$; (b). $\xi = 0.7$; (c). $\xi = 1.0$; (d). $\xi = 1.3$; (e). $\xi = 3.0$. The background color corresponds to different phases: white (hexagonal), gray (disordered), green (dimer lattice), black (stripe), cyan (honeycomb lattice), orange (trimer lattice), purple (tetramer lattice), and blue (kagome lattice). There are two separate disordered 'glassy' phases, GHeS and GHoK, at $\rho \approx 1.00$ and $\rho \approx 2.00$, respectively. The insets show typical configurations for each phase.

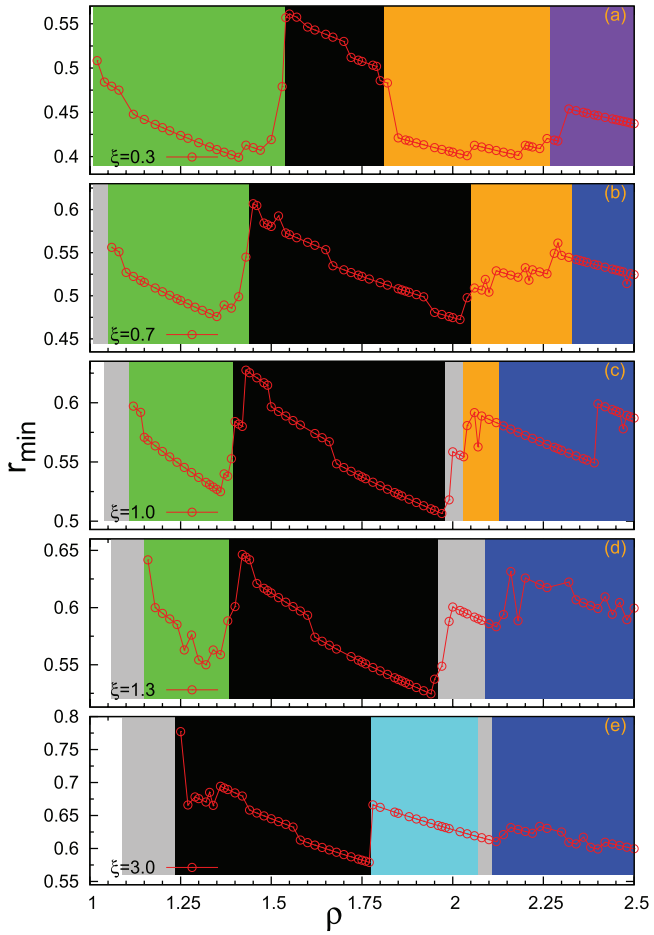

Figure 8. The distance between the nearest neighbor of the vortex r_1 as a function of density ρ. The background colors correspond to the same phases as described in figure 7 and r_1 was determined by the position of the first peak of $g(r)$.

figure 7 clearly indicates that a sharp transition as $n_1 \to 1$ upon entering the dimer lattice phase. The static structure factor shown in figure 6(c) displays a six-fold rotational symmetry. However, at large $\mathbf{k}$ the intensity of the peaks is diminished and the peaks are broadened due to the ordering of the dimers into domains of alignment. As the density and ξ are increased, the dimers in phase III begin to align. At fixed ξ/λ, increasing the density results in a decrease in r_1 (see figure 8) while increasing ξ/λ at fixed ρ results in an increases in r_1 (see figure 9). An example configuration of aligned dimers is shown in figure 10(a).

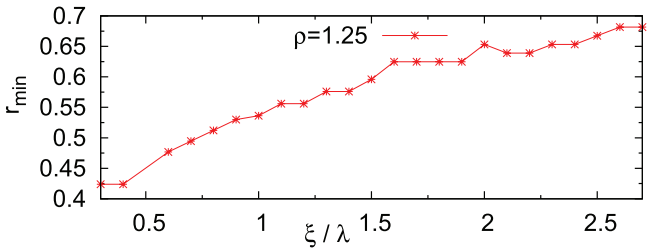

Figure 9. The distance between the nearest neighbor of the vortex r_1 as a function of $\xi/\lambda = 0.3$ to 2.7 at fixed $\rho = 1.25$.

Further increasing the density and/or ξ/λ results in the formation of stripes in the ground state (phase IV). A representative configuration is shown in figure 4(d) and corresponding $g(r)$ and $S(\mathbf{k})$ are plotted in figures 5(d) and 6(d), respectively. From the RDF for $\rho = 1.60$ and $\xi/\lambda = 0.3$, we observe the first peak at $r_1 = 0.546$ and subsequent peaks at $r_2 = 1.093$, $r_3 = 1.171$, and $r_4 = 1.624$. The second and fourth peaks are correlated with the line of vortices in a stripe with $r_2 = 2r_1$ and $r_4 \approx 3r_1$. The third peak, however, describes the distance between neighboring stripes. In the structure factor, we observe a dispersed two-fold symmetry corresponding to the stripe directions. The distance between nearest neighbor r_1 will also decrease as the density increases which was shown in the black section of figure 8.

As the density ρ continues to grow, the stripe phase will transform to honeycomb lattice for $\xi/\lambda > 1.5$, a disordered phase for $1.0 < \xi/\lambda < 1.5$, and a trimer lattice for $\xi/\lambda < 1.0$. The representative snapshot ($\rho = 2.02$ and $\xi/\lambda = 3.9$) for the honeycomb lattice (phase V) is shown in figure 4(e). The radial distribution function (figure 5(e)), the structure factor (figure 6(e)), and nearest neighbor number $n_1 = 3$ are consistent with what is expected for a honeycomb lattice but the phase contains a number of defects that result in a broadening in the peaks of $g(r)$ and $S(\mathbf{k})$.

From $0.2 \leqslant \xi < 1.0$, the stripe will transform to a polarized triangle trimer lattice, which was denoted as phase VII in the phase diagram in figure 3. (The reason why it's called polarized triangle trimer lattice will be discussed later in figure 20.) A representative snapshot and the corresponding RDF and static structure factor $S(\mathbf{k})$ for this phase at $\rho = 2.12$, $\xi/\lambda = 0.3$ are shown in figures 4(g), 5(g) and 6(g), respectively. Similar to a stripe phase, one vortex in a trimer lattice has two nearest neighbors located at a distance r_1 and form an equilateral triangle. Each trimer then forms a hexagonal lattice. Consequently, the RDF has a sharp first peak and subsequent peaks correspond to the distance between vortices in different trimers. The static structure factor $S(\mathbf{k})$ pattern shown in figure 6(g) shows a hexagonal lattice with six voids around one hexagon which is same as the result of perfect trimer lattice created by artificially pinning the vortices [34]. The micro-structure of the polarized triangle trimer lattice is shown in the pinned panel in the orange section in figure 7(a). The nearest neighbor number n_1 changes at different ξ/λ. For $0.2 \leqslant \xi < 0.6$, n_1 will always be 2 which is shown in the orange section in figure 7(a). For $0.6 \leqslant \xi < 1.2$, n_1 will increase from 2 to 3 which is shown in the orange section in figures 7(b)and (c). The reason will be discussed later at the transformation from trimer lattice to kagome lattice. The distance between nearest neighbor r_1 is not always decrease as the density ρ increases which is shown in the orange section in figures 8(a)–(c).

As the density continues to grow, the trimer lattice at $0.2 \leqslant \xi < 0.6$ transforms to a tetramer lattice (phase VIII). The representative snapshot, RDF, and static structure factor $S(\mathbf{k})$ for this phase at $\rho = 2.45$ and $\xi/\lambda = 0.3$ are shown in figures 4(h), 5(h) and 6(h), respectively. In this phase, four vortices will form a rhombus group due to the short-range interaction and the long-range interaction forces the tetramers to order into a hexagonal lattice. In a tetramer, half the vortices have 2 nearest neighbors and half have 3 nearest neighbors, resulting in $n_1 = 2.5$, which can be clearly seen in figure 7(a). The micro-structure of the tetramer lattice is shown in the pinned panel in the purple section in figure 7(a). The distance between nearest neighbor r_1 decreases as the density increases which is shown in the purple section in figure 8(a).

For $0.6 \leqslant \xi < 1.2$ the trimer lattice transforms to a kagome lattice (phase IX). The representative snapshot, RDF, and static structure factor for the kagome lattice at $\rho = 2.50$, $\xi/\lambda = 1.0$ are shown in figures 4(i), 5(i) and 6(i), respectively. In this phase each vortex has 4 nearest neighbors and $g(r)$ features a sharp peak corresponding to the nearest neighbor distance, with subsequent peaks being related to the distances between the second, third, and fourth nearest neighbors.

The transition between the trimer and kagome lattice phases can be understood more clearly by carefully examining the trimer lattice phase. In figure 10(b), we illustrate an individual trimer and its neighbors at $\rho = 2.26$, $\xi = 0.8$, $N_v = 780$. Here, r_1 is the distance between vortices within one trimer and r_2 is the distance between neighboring trimers. As the density increases, the difference between r_1 and r_2 continues to decrease. Once $r_1 = r_2$, the system forms a kagome lattice since each trimer has the same alignment.

The transition from the honeycomb lattice (phase V) to the kagome lattice (phase IX) is separated by a disordered region with characteristics of both the honeycomb and kagome lattices, which will be referred to as GHoK (phase VI). A representative snapshot of this phase at $\rho = 2.08$ and $\xi/\lambda = 2.5$ is shown in figure 4(f). Here, the system forms domains of honeycomb and kagome lattices with the size of the kagome domains increasing as the density increases and the number of nearest neighbors smoothly increasing from $n_1 = 3$ to $n_1 = 4$ (see figure 7). The RDF and static structure factor corresponding to this snapshot are illustrated in figures 5(f) and 6(f). There are no sharp peaks in $g(r)$, shown in figure 5(f), and there are only broad peaks and plateaus with no clear minima. The static structure factor in figure 6(f) shows four uniform rings which suggests that this phase has no broken symmetries and is a disordered phase.

In addition to the disordered phase separating the honeycomb and kagome lattices, there exists a disordered phase separating the hexagonal lattice (phase I), dimer lattice (phase III), and stripe (phase IV) phases, which we will refer to as GHeS (phase II). The transition occurs directly from the hexagonal lattice for $\xi > 0.6$. As the density increases further, the disordered phase transitions to the dimer lattice for $\xi < 2.75$ and the stripe phase for $\xi > 2.75$. A representative snapshot of

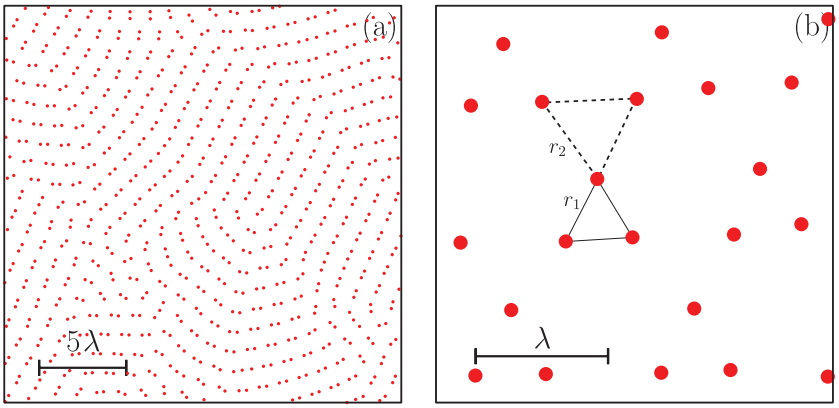

Figure 10. (a) Dimer lattice lined up at $\rho = 1.50$ with $\xi/\lambda = 0.3$. (b) A small fraction of trimer lattice at $\rho = 2.26$, $\xi/\lambda = 0.8$, $N_v = 780$. r_1 is the distance between vortices within one trimer and r_2 is the distance between different trimers. r_1 and r_2 is used to explain the transformation from trimer lattice to kagome lattice.

the GHeS phase at $\rho = 1.12$, $\xi/\lambda = 3.5$ is shown in figure 4(b) and the corresponding $g(r)$ and $S(\mathbf{k})$ are shown in figures 5(b) and 6(b), respectively. From the $g(r)$, we can see that the position of the first peak of GHeS phases, $r/\lambda = 0.97$, is closer than the position of the first peak in hexagonal lattice, $r/\lambda = 1.02$[6]. Note that the peaks in $g(r)$ are much broader than the hexagonal lattice result and that there are plateaus and no single clear minimum between peaks. All of these features suggest that it has no clear local structure. In the static structure factor, there are several rings and no symmetry is broken. The combination of the features in the RDF and the static structure factor indicate that phase II is a frustrated disordered phase. From the representative snapshots in figure 4(b), we note that the hexagonal order has been destroyed and that the system is attempting to form a linear order but there is too much competition for it to occur. In this phase, the number of nearest neighbors varies wildly, either increasing to around 7 or decreasing to around 4 (see figure 7).

Generally, in the phase diagram in figure 3, the long range power law interaction will force the vortices to form a hexagonal lattice at low densities. As the density increases, the short-range repulsive and attractive interactions will dominate with the long-range term, forcing the system to form different phases as the short-range repulsive and attractive terms compete. But there exists a rule: under the pair interaction in figure 1, the short range interaction will force the system to form a higher nearest neighbor number n_1 phase as the density ρ increases. Moreover, the presence of the long-range power law term enhances long-range ordering of the local patterns. When the density increases significantly, the short-range repulsive term becomes especially important resulting in a frustrated kagome lattice.

However, when the attractive term is enhanced by increasing ξ above a critical ξ_c, it dominates the other interactions resulting in a cluster phase (phase X). The cluster phase is denoted as phase X in the phase diagram in figure 3. Note that the power long-range repulsion caused by stray fields still plays an important role in causing clusters to order into a hexagonal 'super-lattice'], which is illustrated in figure 4(j) for $\rho = 0.25$, $\xi/\lambda = 5.0$ and $N_v = 2958$. The value of ξ_c is dependent on the density, increasing from $\xi_c = 3.3$ at very small densities to $\xi_c = 4.3$ at $\rho \geqslant 0.62$.

For $4.3 \leqslant \xi/\lambda \leqslant 10.0$, the ground state of the vortex system is the cluster. For $3.4 < \xi < 4.3$, the potentials have an attractive well, but the final configuration of vortex is not the cluster for large densities ($\rho \geqslant 0.62$). The system structure is strongly affected by multiple repulsive length scales. For low densities $0.05 < \rho \leqslant 0.12$, the weak attractive interaction is important and the vortices can form a cluster. When the density increases, the distance between vortices decreases, and the short strong repulsive interaction will dominate and force vortices to form the normal vortex lattice.

The cluster phase exhibits a nontrivial dependence on the system size. If number of vortices in the simulation is small, then the ground state of the system will be a single cluster, shown in figure 11 for $\rho = 2.37$ and $\xi/\lambda = 9.0$. Note that the RDF for a ground state with multiple clusters (figure 5(j)) and structure factor (figure 6(j)) is the same as the structure for a single cluster (figure 11). If number of vortices in the simulation is large enough, multiple clusters will be the ground state, i.e. there is a maximum size of one cluster. For example, at $\rho = 0.25$, $\xi/\lambda = 5.0$, the system with 780 vortices will form one cluster, but the system with 2958 vortices will form multiple clusters phase.

Here the interior of each cluster is densely packed into a hexagonal lattice with the density decreasing as one moves outward toward the edge of the cluster, which is a single ring of vortices equally spaced. However, the interior structure of the cluster can exhibit voids, stripes, and other complex structures [27].

Near the ξ_c boundary, if the system size is too small, the system will instead feature a large, non-uniform stripe phase. Here we illustrate a typical vortex configuration, RDF, and structure factor in figure 12 for $\rho = 2.37$, $\xi/\lambda = 4.75$ and $N_v = 2958$. The RDF of middle phase is the same as the RDF of cluster phase in figure 5(j). And $S(\mathbf{k})$ pattern is similar to the multiphase cluster phase in figure 6(j). The interesting result is that when the vortices number increases to $N_v = 4012$, the whole system will form a big single cluster. If the vortices number is too small, such as $N_v = 986$, 2016, the ground state of the whole system will be the same as the low ξ case. For example,

[6] See footnote 5.

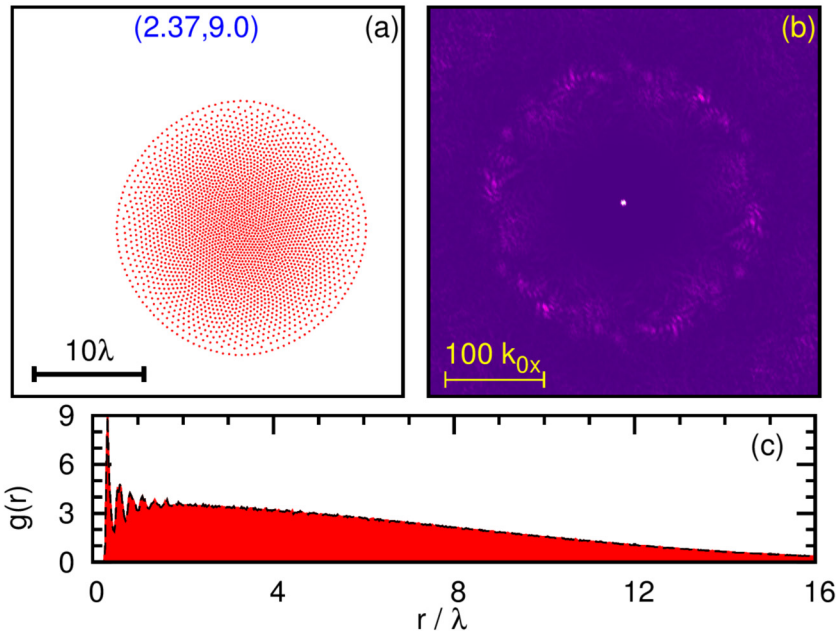

Figure 11. The (a) vortex configuration, (b) static structure factor, and (c) RDF of a single cluster with $\rho = 2.37$, $\xi/\lambda = 9.0$, and $N_v = 2958$.

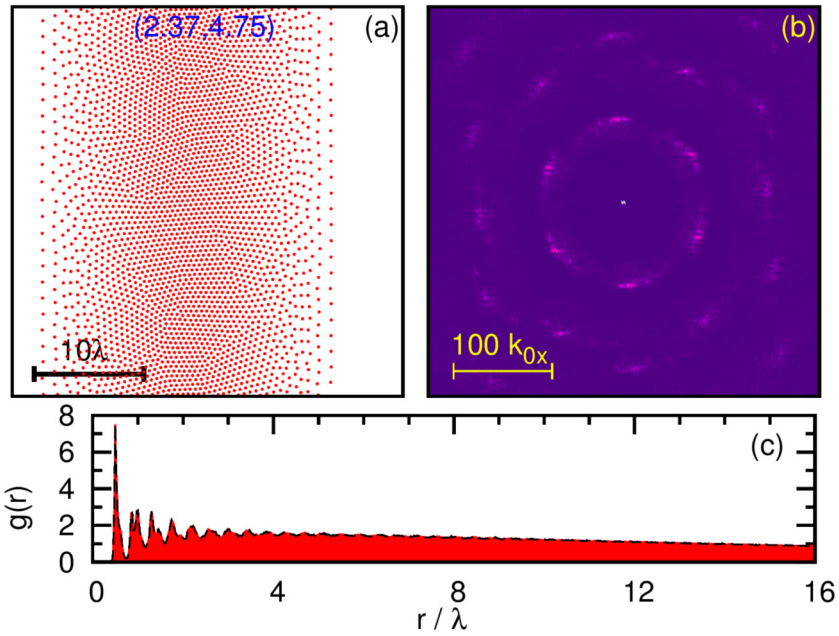

Figure 12. The (a) vortex configuration, (b) static structure factor and (c) RDF of the non-uniform stripe phase at $\rho = 2.37$, $\xi/\lambda = 4.75$, and $N_v = 2958$. When the vortices number increases to $N_v = 4012$, the whole system will form a circular cluster.

at $\rho = 2.37, \xi/\lambda = 4.75$, if $N_v = 2016$, the ground state of system is kagome lattice (snapshot is shown in figure 4(i)) which is the same as $\xi < \xi_c$ case. When $N_v = 2958$, it forms the cluster middle phase in figure 12(a). Once the system size reaches $N_v = 4012$, the ground state of the system becomes a single cluster shown in figure 11(a) and increasing the system size further results in multiple clusters. This occurs due to long-range repulsive interaction mediated by stray fields.

There is additional area of the phase diagram where behavior for the very small density $\rho = 0.05$ is not reproducible for larger densities. At $\rho = 0.05$, as ξ/λ increases, the system transforms from a hexagonal lattice to a void phase at $\xi/\lambda = 3.3$ to 3.4, illustrated in figure 13. When the number of vortices is increased, the system instead forms the cluster middle phase and cluster phase described above.

4.2. Phase diagram II

The ground state phase diagram in the ρ-ξ/λ plane corresponding to figure 2 is shown in figure 14. The main difference with the potential of figure 1 is the presence of a small plateau located between $r/\lambda = 1.0$ and 2.0, resulting in a complex phase diagram with 17 phases overall. As in our discussion on the previous phase diagram, we represent each

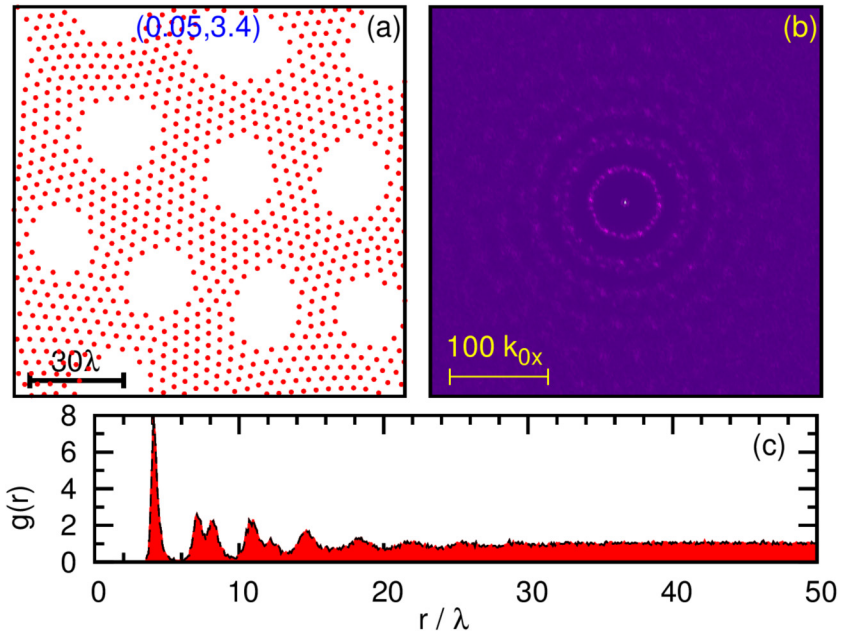

Figure 13. The (a) vortex configuration, (b) static structure factor, and (c) RDF of the void phase at $\rho = 0.05$, $\xi/\lambda = 3.4$, and $N_v = 780$.

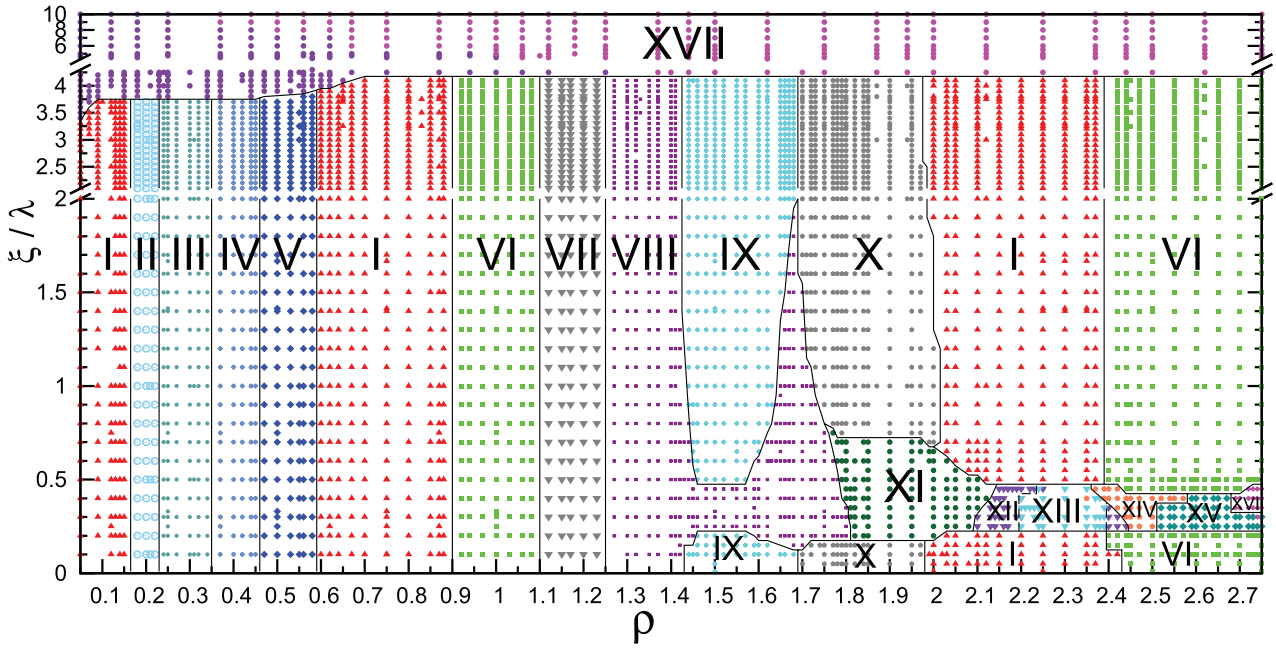

Figure 14. Phase diagram of the final vortex configuration at zero temperature in the ξ/λ and density ρ plane for the potentials shown in figure 2. There are 17 phases in this phase diagram. The Roman numerals in every section denote every phase. The snapshot, RDF, and static structure factor of a representative final configuration for each phase is shown in figures 15–17, respectively.

phase with a colored symbol. Phase I is the hexagonal lattice (solid red up-pointing triangle), phase II is an unaligned dimer lattice (sky blue empty circle), and phase III is a stripe (cadet blue solid circle). Phase IV is a void state (purple solid rhombus) and phase V is a hexagonal lattice with voids (solid blue rhombus). Phases VI and VIII are a square lattice (solid green square) and an aligned dimer lattice (magenta solid square), respectively, while phase VII is a disordered phase separating the two (solid gray down-pointing triangle). Phase IX is a honeycomb lattice (solid cyan rhombus) and phase X is an intermediate phase between the honeycomb and hexagonal lattice phases (solid gray pentagon). Phase XI is a dimer stripe (solid dark green circle), phase XII is a linear trimer hexagonal lattice (solid violet down-pointing triangle), and phase XIII is a trimer lattice (solid cyan down-pointing triangle). Phases XIV, XV, and XVI are the zig-zag stripe (solid coral pentagon), trimer stripe (solid turqoise diamond), and tetramer stripe (solid fuschia diamond) phases, respectively. Finally, phase XVII is a cluster phase (solid pink circle).

We show the snapshot of a representative final configuration for each phase in figure 15, the corresponding RDF in

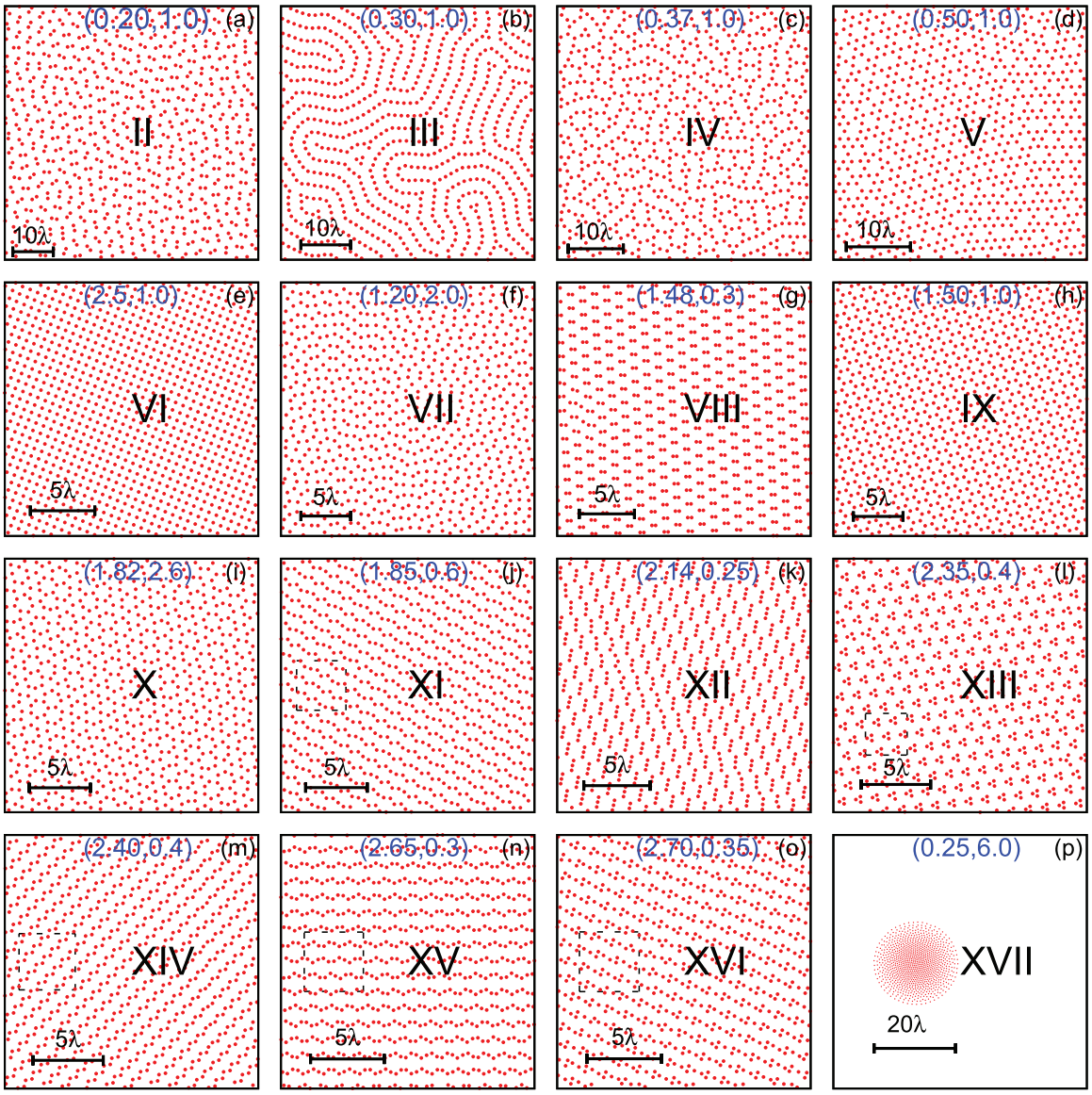

Figure 15. Snapshots of a representative vortex configuration for each phase (indicated by Roman numerals) in figure 14.

figure 16, and the corresponding static structure factor $S(\mathbf{k})$ pattern in figure 17. The number of the nearest neighbors n_1 in the different phases are shown in figure 18. With the exception of the hexagonal lattice phase, note that the background color in figure 18 corresponds to the color of the point used in figure 14. Here we show the n_1 for $\xi = 0.4$, 0.6, 1.0, and 3.0, which is sufficient to show all of the phase transitions in figure 14.

First, similar to phase diagram I in figure 3, this system features a critical ξ_c. When $\xi > \xi_c$, the system forms giant clusters since the attractive interaction becomes dominant, with the long-range power law repulsion resulting in individual clusters forming a hexagonal lattice. Here, ξ_c will increase from $\xi_c = 3.4$ at $\rho = 0.05$ to $\xi_c = 3.75$ at $\rho = 0.46$, then stabilizes to $\xi_c = 4.2$ for $\rho \geqslant 0.7$. The cluster phase is denoted as phase XVII in the phase diagram in figure 14. The snapshot, RDF, and static structure factor of a typical cluster phase are shown in figures 15(p), 16(p) and 17(p), respectively. As with the previous phase diagram, if the number of vortices is small at fixed ρ and ξ/λ, the system will form a single giant cluster which will become a lattice of clusters as N_v is increased. Similar to phase diagram I, there is also the cluster middle and void phase near the boundary ξ_c.

Below ξ_c, there are sixteen vortex phases in the phase diagram. At very low density, $0.05 \leqslant \rho < 0.16$, from $\xi = 0.1$ to 3.4, the ground state will be a hexagonal lattice (phase I). For this phase, the dominant interaction is the long-range repulsive power law term. Here, the snapshot, RDF, and static structure factor of a typical configuration are no different from the results shown previously in figures 4(a), 5(a) and 6(a), respectively. Also, we can confirm that the number of nearest neighbors in this phase is 6 (see figure 18).

As the density increases, the competition between different length scales will form an dimer lattice (phase II) at $\rho = 0.17$ to 0.23. The snapshot of a typical configuration is shown for $\rho = 0.2$ and $\xi/\lambda = 1.0$ in figure 15(a). Here we note that although the vortices pair and form a lattice, the orientation of each dimer varies throughout the system. Consequently,

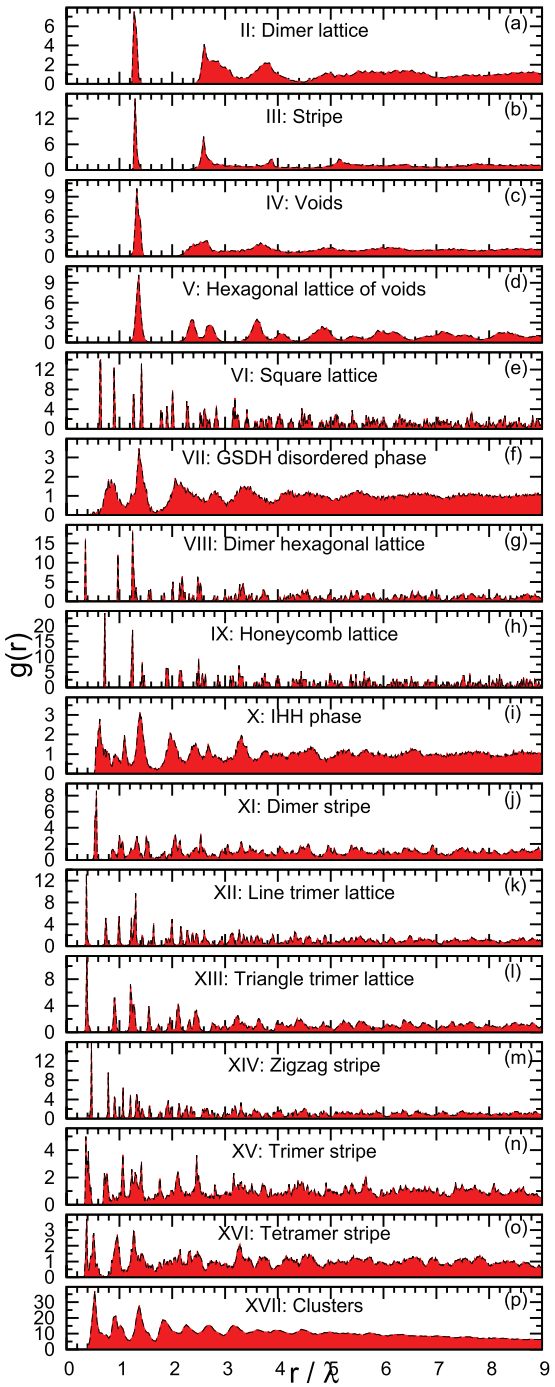

Figure 16. Radial distribution function $g(r)$ for phases illustrated in figure 15.

the number of nearest neighbors decreases to 1 in this phase and there is a very sharp beak in $g(r)$ (see figure 16(a)). Due to the random orientation of the dimers, $S(\mathbf{k})$ has a uniform ring (see figure 17(a)), reminiscent of the disordered phases of figure 3.

As the density continues to increase, the dimers will line up and forming stripes (phase III). In figure 15(b), we show a typical stripe configuration for at$\rho = 0.3$ and $\xi/\lambda = 1.0$. Because the stripes do not order uniformly, the RDF and static structure factor do not show strong signatures of phase IV of figure 14. In the RDF, the peaks in figure 16(b) are broadened in comparison to figure 5(d). Moreover, the static structure factor in figure 17(b) has a uniform ring structure instead of the strong signal in figure 6(d).

Next, the system transitions to a void phase (phase IV). A typical configuration for this phase is shown in figure 15(c) for $\rho = 0.37$ and $\xi/\lambda = 1.0$. Here, the system is attempting to form dimers, trimers, and tetramers but the system is too densely packed to for it to be possible with n_1 varying between 3 and 4 (see figure 18). Consequently, the only features visible in the RDF in figure 16(c) are due to short range pairing and the static structure factor in figure 16(c) has a uniform ring structure.

As density ρ increases from 0.46 to 0.59, the system will form a hexagonal lattice with voids (HLV) which is denoted as phase V in figure 14. Correspondingly, n_1 will increase from 4 to 6 which is shown in figure 18, with $n_1 \sim 5$ around density $\rho = 0.55$. The snapshot of the HLV phase is shown in figure 15(d).

As the density increases, the number of the empty sites will decrease until the system transforms to a hexagonal lattice. The corresponding RDF and static structure factor $S(\mathbf{k})$ of HLV is shown in figures 16(d) and 17(d). Note that $g(r)$ for this phase is consistent with the hexagonal lattice shown in figure 5(a) and there is a six-fold symmetry in $S(\mathbf{k})$.

From figure 18, we can find that there is not a very sharp difference in n_1 between dimer, stripe, voids, and HLV phases. Their nearest neighbor number n_1 increases continuously from 1 to 6 and the order of the phases in this part of the phase diagram is consistent with what is expected for a system exhibiting a purely repulsive interaction [35].

Increasing the density further results in a transition from the hexagonal lattice to a square lattice (phase VI), where $n_1 = 4$. A typical configuration is shown in figure 15(e). The corresponding RDF and static structure factor for the square lattice are shown in figures 16(e) and 17(e), respectively. In both $g(r)$ and $S(\mathbf{k})$, the peaks are very sharp, indicating that there is very little disorder in the system.

Next, the system transitions to a disordered phase (phase VII) from $\rho = 1.10$ to $\rho = 1.25$ due to the competing interactions. Since this phase separates the square lattice and a dimer hexagonal lattice, we shall refer to this phase as GSDH. A typical snapshot and corresponding RDF and $S(\mathbf{k})$ are shown in figures 15(b), 16(f) and 17(f), respectively. As with the previous disordered phases, the features in $g(r)$ are very broad, indicating a lack of local structure, and the structure factor has a uniform ring with no broken symmetries.

From $\rho = 1.25$ to 1.43, the ground state of system will form a dimer hexagonal lattice (phase VIII). The snapshot, RDF and static structure factor $S(\mathbf{k})$ for this phase at $\rho = 1.48$ and $\xi/\lambda = 0.3$ are shown in figures 15(g), 16(g), and figure 17(g). Unlike phase II, the dimers lattice in phase VIII have a universal polarization, resulting in sharper peaks in $g(r)$. Contrasting with figure 6(c), which has a six-fold symmetry in $S(\mathbf{k})$, the static structure factor of phase VIII features a broken symmetry along the k_x direction.

As the density ρ continues to increase, the ground state of system depends on ξ/λ and can be split into two regions. The

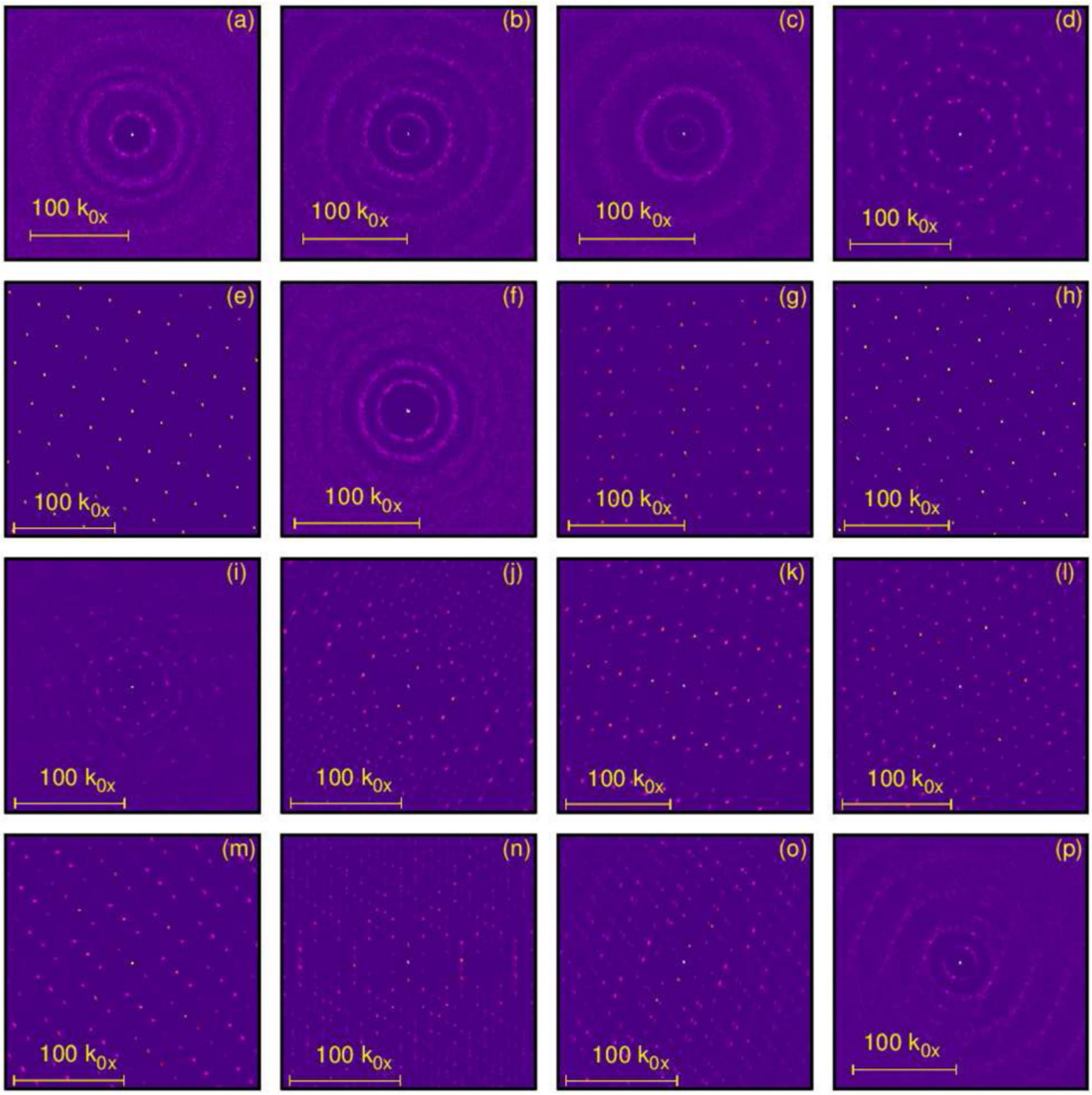

Figure 17. Static structure factor $S(\mathbf{k})$ for phases illustrated in figure 15.

first region has both large and small ξ while the second has intermediate ξ from $\xi \approx 0.2$ to $\xi \approx 0.5$. For convenience, we will denote these as regions I and II, respectively.

Let us first consider the transitions in region I. As the density is increased while in the dimer hexagonal lattice phase (phase VIII), the distance between dimers gradually decreases until the dimer–dimer distance is equal to the distance between vortices inside a dimer, resulting in a honeycomb lattice (phase IX). The snapshot, RDF and static structure factor $S(\mathbf{k})$ of this phase for $\rho = 1.50, \xi/\lambda = 1.0$ is shown in figures 15(h), 16(h) and 17(h), respectively. The nearest neighbor number n_1 for region I is shown in panels (b), (c), and (d) of figure 18 and is consistent with the expected value of $n_1 = 3$.

Increasing the density further results in an intermediate phase (IHH for short) is denoted as phase X in figure 14. A typical configuration is shown in figure 15(i) for $\rho = 1.82$ and $\xi/\lambda = 2.6$. It is immediately clear that there is no local structure, which is confirmed by the lack of sharp peaks in the RDF (see figure 16(i)). However, the phase does retain a six-fold symmetry in $S(\mathbf{k})$ instead of the ring structure one would expect for a disordered/glassy phase. As the density in this phase is increased, the number of nearest neighbors increases from $n_1 = 3$ to $n_1 = 5$.

As mentioned previously, phase X transitions to a hexagonal lattice (phase I) as the density is increased. Increasing the density further results once again in a transition to a square lattice (phase VI).

In region II, the dimer hexagonal lattice (phase VIII) transitions to a dimer stripe (phase XI) phase, which is depicted in figure 15(j) for $\rho = 1.85$ and $\xi/\lambda = 0.6$. In this phase, $n_1 = 2$ and the orientation of the dimers is not consistent. This can be clearly seen in figure 19(a), which is an enlargement of the dashed box in the configuration of figure 15(j). The RDF for this configuration is shown in figure 16(j) and features a sharp peak in connection with the pairing, while subsequent peaks are broadened due to the varying orientation of the dimers. The static structure factor (figure 17(j)) exhibits a two-fold symmetry.

Next, the system transitions to a linear trimer lattice (phase XII). A typical configuration is shown in figure 15(k)

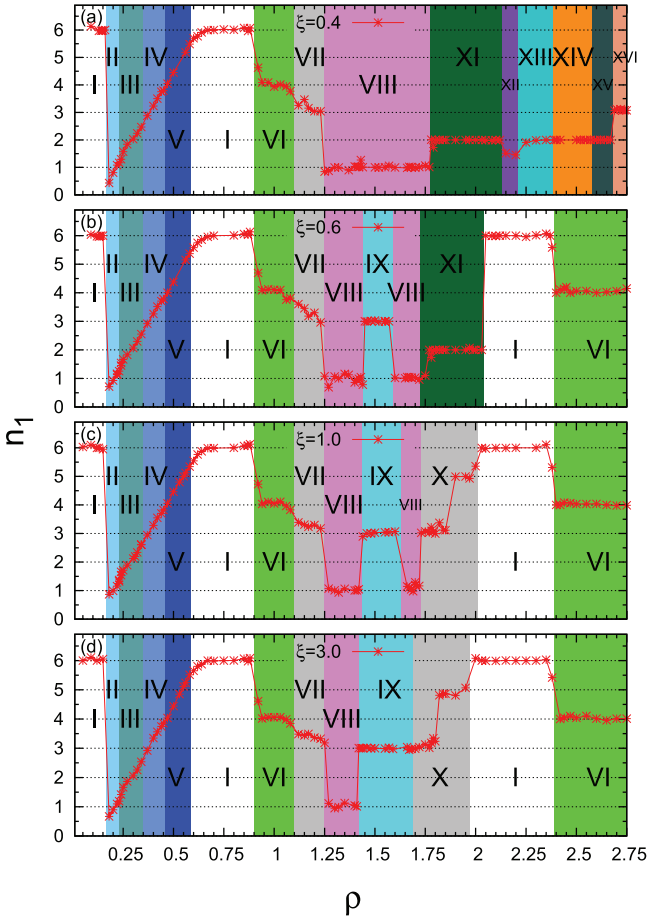

Figure 18. Nearest neighbor number n_1 at (a). $\xi = 0.4$, (b). $\xi = 0.6$, (c). $\xi = 1.0$, and (d). $\xi = 3.0$. The background color corresponds to the color used for the phase in figure 14 and each phase is labeled by the appropriate Roman numerals as well.

for $\rho = 2.14$ and $\xi/\lambda = 0.25$. Unlike the dimer lattice phase, each linear trimer is aligned with its neighbors. Consequently, the features in the RDF and static structure factor are much sharper, as can be seen in figures 16(k) and 17(k), respectively. Additionally, the vortices in each trimer do not have the same number of nearest neighbors, with the vortex in the center having 2 neighbors while the vortices on the ends only having one, resulting in $n_1 \approx 4/3$ (see figure 18(a)).

The next transition is to aligned triangular trimer lattice (phase XIII). A representative configuration is shown in figure 15(l). Here, we contrast this phase with the triangle trimer lattice of phase diagram I (phase VII in figure 3), showing a close up view of figure 4(g) in figure 20(a) and a close up view of figure 15(l) in figure 20(b). The size of dashed box in figures 4(g) and 15(l) is $3\lambda \times 3\lambda$. The main difference between the two phases is the alignment of the trimers, which is illustrated with a solid black line (there are three equivalent ways to define the orientation axis for a trimer). The trimer of phase diagram I is aligned to the midpoint between neighboring trimers while the trimer of phase XIII in phase diagram II is aligned to neighboring trimers. Since there is a $\theta = \pi/6$ angle between the orientation of trimer with the alignment direction of trimers in figure 20(a), we called this phase polarized triangle trimer lattice. Note that the RDF and static structure factor of both phases are similar and the number of nearest neighbors is $n_1 = 2$. Note that the aligned triangle trimer lattice is similar to states of colloidal molecular crystal in the presence of periodic substrate [34, 40–43]. Another phenomenon is that the linear trimer and aligned triangle trimer lattice are extremely close in energy and are nearly degenerate. In the region with $2.40 < \rho < 2.45$ and $0.25 < \xi/\lambda < 0.40$, the linear trimer has an energy that is less than 0.01% smaller than the triangular trimer lattice.

This phenomenon, different initial configuration can get different stable state at the same condition, happens at several other places. For example, at $\rho = 2.75$, $\xi/\lambda = 0.25$ and 0.30, the tetramer stripe(phase XVI in figure 14) and trimer stripe(phase XV in figure 14) can both be the stable state based on different initial configuration. At $\xi/\lambda = 0.25$, the energy of trimer stripe is 0.001 03% smaller than the tetramer stripe.

Next, the system transitions to a zig-zag stripe phase (phase XIV). A typical configuration is shown in figure 15(m) for $\rho = 2.40$ and $\xi/\lambda = 0.4$. In this zig-zag phase, there are two vortices between each bend and the number of nearest neighbors is $n_1 = 2$. A close up view of this phase is shown in figure 19(b) and the angle between nearest neighbours was calculated to be $\theta \approx 116°$. The RDF and static structure factor for this phase are shown in figures 16(m) and 17(m).

Increasing the density further results in a transformation to a trimer stripe phase (phase XV). The snapshot, RDF, and static structure factor $S(\mathbf{k})$ for this phase at $\rho = 2.65$ and $\xi/\lambda = 0.3$ are shown in figures 15(n), 16(n) and 17(n), respectively. The nearest neighbor number $n_1 = 2$ in figure 18 and we illustrate a section of the phase in figure 19(c). Here, each stripe is comprised of both dimers and linear trimers to form zig-zags of varying depth. The structure factor of this phase also features a two-fold symmetry like the dimer stripe case in figure 17(j).

The final phase in region II is a tetramer stripe (phase XVI). The snapshot, RDF, and static structure factor for the the tetramer stripe at $\rho = 2.70$ and $\xi/\lambda = 0.35$ are shown in figures 15(o), 16(o) and 17(o), respectively. Here, each stripe is mostly comprised of tetramers with the occasional triangular trimer. The RDF for this phase features two peaks that are very close in distance and $S(\mathbf{k})$ features a two-fold symmetry since it's a stripe phase in the large scale.

In order to clarify the distance between the nearest neighbor in this phase, we marked six vortices as A, B, C, D, E and F. Vortices B,C,D,E form a tetramer in figure 19(d). For example, vortex C as the center, the distance CE is equal to CD and a little bit smaller than CB. This slightly difference between CE(CD) and CB cause the first peak of its RDF in figure 16(o) forks two very close peaks. We recognize the first two very close peaks as the first peak and count the vortices within it as its nearest neighbors. The nearest neighbor can be recognized as the following: vortex B's nearest neighbors are A, C, and E; vortex C's nearest neighbors are B, D, and E; vortex D's nearest neighbors are C, E, and F. Therefore, every vortex has three nearest neighbors, which we illustrate in figure 18(a).

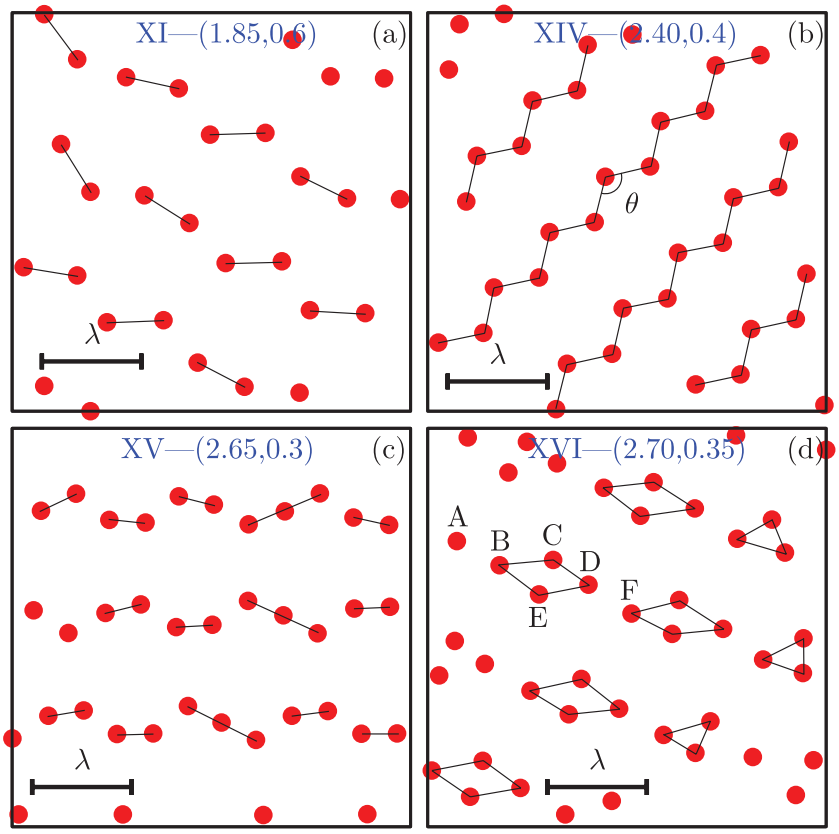

Figure 19. The enlarged dash box in: (a) phase XI in figure 15(j); (b) Phase XIV in figure 15(m); (c) Phase XV in figure 15(n); (d) Phase XVI in figure 15(o). We use the black line to link the vortices to show the micro-structure of the phase.

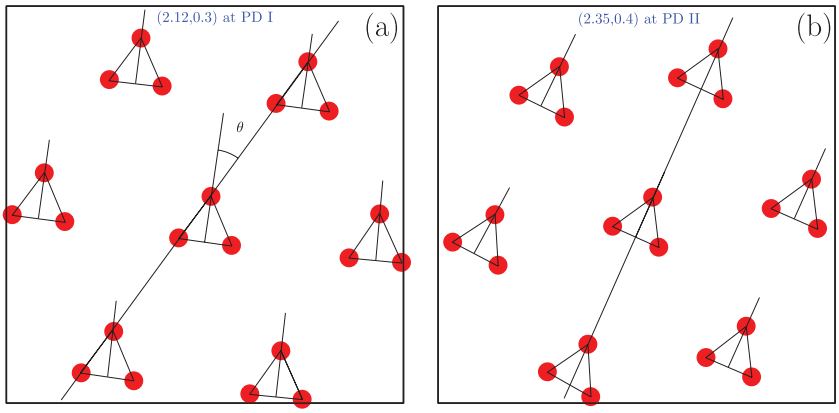

Figure 20. Comparison of the trimer lattices is found in (a) figure 3 (Phase VII) with $\rho = 2.12$ and $\xi/\lambda = 0.3$ and (b) figure 14 (Phase XIII) with $\rho = 2.35$ and $\xi/\lambda = 0.4$. The size of this box is $3\lambda \times 3\lambda$. We illustrate individual trimers with a solid black line and indicate the orientation of each trimer. In panel (a), $\theta = \frac{\pi}{6}$, the trimers are aligned to the midpoint between neighboring trimers while in panel (b), $\theta = 0$, the dimers are aligned to neighboring trimers.

5. Discussion

Layered superconducting systems can have inter-vortex forces with several repulsive and attractive length scales. We investigated structure formation in a model system with multiple repulsive and attarctive length scales. Some of them such as hexagonal, square, honeycomb and kagome lattice have been reported [12]. Here we found other new symmetric phases: dimer hexagonal lattice in figure 15(g), linear trimer lattice in figure 15(k), polarized triangular trimer lattice in figure 4(g) and aligned triangular trimer lattice in figure 15(l).

In addition to conventional lattice phases, we observed a hexagonal lattice with voids (figure 15(d)) and various stripe phases with different unit cells: a dimer stripe (figure 15(j)), a zigzag stripe (figure 15(m)), a trimer stripe (figure 15(n)), and a tetramer stripe (figure 15(o)). Next, several very stable disordered states with no clear local structure were found in molectular dynamics sumulations. On the other hand, some of the very stable phases, e.g. dimer phase in figure 15(a), stripe in figure 15(b) and voids in figure 15(c), are disordered in the intermediate and long range scale while having a local structure.

With the same local structure, different arrangements of local structure can form different phases which will affect the property in the intermediate and long-range scales. For example, there are several types of dimer lattices based on different dimer orientation. Dimers can locally form hexagonal lattice in a domain in the phase III in figure 4(c). Dimers can also be disordered in the phase II in figure 15(a). All of the dimers can have a universal orientation and form a hexagonal lattice in phase VIII of figure 15(g). Dimers can also line up to form a stripe (figure 10(a)).

Finally, there are three types of trimer lattice with different arrangement of trimers in this system. Three vortices can form two types of trimer: linear trimer (shown in figures 15(k)) and two types of triangluar trimers (shown in figure 4(g) and 15(l)). The angle θ between the orientation of triangular trimers and the alignment direction of triangle trimers can be different in various arrangements. In the phase VII in figure 4(g) (close up view in figure 20(a)), $\theta = \pi/6$, it formed a polarized triangular trimer. In the phase XIII in figure 15(l) (close up view in figure 20(b)), $\theta = 0$, it formed an aligned triangular trimer lattice.

6. Summary

In conclusion, quantum vortices in superconductors may offer a unique route for engineering magnetic field configurations required for quantum emulators. This application demands creation of various geometries of vortex matter which is not possible in type-2 superconductors in the absence of pinning center.

Here we propose to utilize type-1.5 superconductors which possess several attractive and repulsive length scales in the intervortex interaction potential. Several repulsive lengths scales can be engineered in layered structures, where difference layers have different magnetic penetration lengths or in superconductor-insulator multilayers where magnetic field lines can spread in the insulating layers due to suppression of the Meissner effect.

We studied this situation utilising a model of point-particles with effective interaction potential. This model neglects non-pairwise intervortex forces, which in fact are small under certain conditions [18]. In case of the realization in layered system the applicability of the point-particle model assumes high vortex line tension which makes the system translationally invariant in z-direction. We demonstrated that in such systems it is possible to realize a wide range of vortex states. Recent study of the vortex cluster phase in type-1.5 superconductors, similar to the ones considered here, demonstrated that the disordered vortex clusters states have glass dynamics [44].

Acknowledgments

This work was supported by the National Science Foundation under the CAREER Award DMR-0955902, Goran Gustafsson Foundation and by the Swedish Research Council 642-2013-7837. QM wants to thank the inspired discussion with Gregory M Grason.

References

[1] Romero-Isart O, Navau C, Sanchez A, Zoller P and Cirac J I 2013 *Phys. Rev. Lett.* **111** 145304
[2] Aegerter C M, Lloyd S H, Ager C, Lee S L, Romer S, Keller H and Forgan E M 1998 *J. Phys.: Condens. Matter* **10** 7445
[3] Riseman T M *et al* 1998 *Nature* **396** 242
[4] Ray S J, Gibbs A S, Bending S J, Curran P J, Babaev E, Baines C, Mackenzie A P and Lee S L 2014 *Phys. Rev.* B **89** 094504
[5] Moshchalkov V, Woerdenweber R and Lang W 2010 *Nanoscience and Engineering in Superconductivity* (Berlin: Springer)
[6] Baert M, Metlushko V V, Jonckheere R, Moshchalkov V V and Bruynseraede Y 1995 *Phys. Rev. Lett.* **74** 3269
[7] Moshchalkov V V, Baert M, Metlushko V V, Rosseel E, Van Bael M J, Temst K, Jonckheere R and Bruynseraede Y 1996 *Phys. Rev.* B **54** 7385
[8] Rosseel E, Van Bael M, Baert M, Jonckheere R, Moshchalkov V V and Bruynseraede Y 1996 *Phys. Rev.* B **53** R2983
[9] Grigorenko A N *et al* 2001 *Phys. Rev.* B **63** 052504
[10] Grigorenko A N, Bending S J, Van Bael M J, Lange M, Moshchalkov V V, Fangohr H and de Groot P A J 2003 *Phys. Rev. Lett.* **90** 237001
[11] Berdiyorov G R, Milošević M V and Peeters F M 2006 *Phys. Rev.* B **74** 174512
[12] Meng Q, Varney C N, Fangohr H and Babaev E 2014 *Phys. Rev.* B **90** 020509
[13] Babaev E and Speight M 2005 *Phys. Rev.* B **72** 180502
[14] Silaev M and Babaev E 2011 *Phys. Rev.* B **84** 094515
[15] Silaev M and Babaev E 2012 *Phys. Rev.* B **85** 134514
[16] Garaud J, Agterberg D F and Babaev E 2012 *Phys. Rev.* B **86** 060513
[17] Carlström J, Garaud J and Babaev E 2011 *Phys. Rev.* B **84** 134518
[18] Carlström J, Garaud J and Babaev E 2011 *Phys. Rev.* B **84** 134515
[19] Babaev E, Carlström J and Speight M 2010 *Phys. Rev. Lett.* **105** 067003
[20] Moshchalkov V, Menghini M, Nishio T, Chen Q H, Silhanek A V, Dao V H, Chibotaru L F, Zhigadlo N D and Karpinski J 2009 *Phys. Rev. Lett.* **102** 117001
[21] Gutierrez J, Raes B, Silhanek A V, Li L J, Zhigadlo N D, Karpinski J, Tempere J and Moshchalkov V V 2012 *Phys. Rev.* B **85** 094511
[22] Dao V H, Chibotaru L F, Nishio T and Moshchalkov V V 2011 *Phys. Rev.* B **83** 020503
[23] Hicks C W, Kirtley J R, Lippman T M, Koshnick N C, Huber M E, Maeno Y, Yuhasz W M, Maple M B and Moler K A 2010 *Phys. Rev.* B **81** 214501
[24] Kawasaki I, Watanabe I, Amitsuka H, Kunimori K, Tanida H and Ōnuki Y 2013 *J. Phys. Soc. Japan* **82** 084713
[25] Fujisawa T, Yamaguchi A, Motoyama G, Kawakatsu D, Sumiyama A, Takeuchi T, Settai R and Ånuki Y 2015 *Japan. J. Appl. Phys.* **54** 048001
[26] Carlström J, Babaev E and Speight M 2011 *Phys. Rev.* B **83** 174509
[27] Varney C N, Sellin K A H, Wang Q Z, Fangohr H and Babaev E 2013 *J. Phys.: Condens. Matter* **25** 415702
[28] Komendová L, Milošević M V and Peeters F M 2013 *Phys. Rev.* B **88** 094515
[29] Pearl J 1964 *Appl. Phys. Lett.* **5** 65
[30] Malescio G and Pellicane G 2004 *Phys. Rev.* E **70** 021202
[31] Glaser M A, Grason G M, Kamien R D, Komrlj A, Santangelo C D and Ziherl P 2007 *Europhys. Lett.* **78** 46004
[32] Olson Reichhardt C J, Reichhardt C and Bishop A R 2010 *Phys. Rev.* E **82** 041502

[33] Olson Reichhardt C J, Reichhardt C and Bishop A R 2011 *Phys. Rev.* E **83** 041501
[34] Reichhardt C and Olson Reichhardt C J 2012 *Phys. Rev.* E **85** 051401
[35] Malescio G and Pellicane G 2003 *Nat. Mater.* **2** 97
[36] Spivak B and Kivelson S A 2004 *Phys. Rev.* B **70** 155114
[37] Parameswaran S A, Kivelson S A, Rezayi E H, Simon S H, Sondhi S L and Spivak B Z 2012 *Phys. Rev.* B **85** 241307
[38] Fangohr H, Cox S J and de Groot P A J 2001 *Phys. Rev.* B **64** 064505
[39] Imperio A and Reatto L 2006 *J. Chem. Phys.* **124** 164712
[40] Reichhardt C and Olson C J 2002 *Phys. Rev. Lett.* **88** 248301
[41] Brunner M and Bechinger C 2002 *Phys. Rev. Lett.* **88** 248302
[42] Agra R, van Wijland F and Trizac E 2004 *Phys. Rev. Lett.* **93** 018304
[43] Arlah A, Franosch T and Frey E 2005 *Phys. Rev. Lett.* **95** 088302
[44] Diaz-Mendez R *et al* 2016 arXiv:1605.00553